

CuNO₂ and Cu⁺NO₂ Revisited: A Comparative ab Initio and DFT Study

Stepan Sklenak* and Jan Hrušák

J. Heyrovsky Institute of Physical Chemistry, Academy of Sciences of the Czech Republic, Dolejskova 3, 18223 Prague, Czech Republic

Received August 10, 2005

Abstract: We have reinvestigated CuNO₂ and Cu⁺NO₂ at ab initio as well as at pure and hybrid DFT levels of approximation employing large ANO basis sets. The systems were fully optimized using the CCSD(T), QCISD(T), BPW91, PBE, PBE0, and B3LYP methods. Several stationary points (minima and transition structures) were found on the related potential energy surfaces (PES). The C_{2v} bidentate η²-O,O isomer is calculated to be the most stable species on the CuNO₂ PES, followed by two monodentate isomers—the C_s η¹-O and C_{2v} η¹-N species which are higher in energy by 12 and 14 kcal/mol, respectively, at CCSD(T)/Basis-II (where Basis-II is 21s15p10d6f4g/8s7p5d3f2g for Cu; 14s9p4d3f/5s4p3d2f for O and N). On the Cu⁺NO₂ PES, the C_s monodentate η¹-O trans (0 kcal/mol) and cis (+3 kcal/mol at CCSD(T)/Basis-II) isomers are found, followed by the C_{2v} monodentate η¹-N isomer (+14 kcal/mol at CCSD/Basis-II). In contrast to the pure DFT, the hybrid DFT methods perform reasonably well for predicting the relative stabilities (except for η¹-N of CuNO₂) and structures; however, their predictions of the bond dissociation energies are less reliable (for CuNO₂ the difference is as much as 10 kcal/mol compared to the CCSD(T) values). The performance of the QCISD(T) method was analyzed, and, furthermore, the issue of symmetry breaking was investigated.

1. Introduction

Nitrogen oxides are important industrial pollutants which can be removed from air by a selective catalytic reduction¹ (SCR) on transition-metal zeolites. Copper is often employed in these processes.^{2–8} Furthermore, it was demonstrated in many studies that the monovalent Cu⁺ ion is the core of the active sites of copper zeolite catalysts.^{9–12} The mechanism of the SCR is not fully understood yet. However, it is plausible to assume that a key role is played by the CuNO₂ complex.

There are different ways¹³ in which NO₂ can coordinate to Cu or Cu⁺. NO₂ can act as a monodentate ligand and coordinate through either O (η¹-O coordination) or N (η¹-N coordination). It can also act as a bidentate ligand and interact with the copper via either two O atoms (η²-O,O coordination) or O and N atoms (η²-O,N coordination). Several theoretical studies of the CuNO₂ system in the gas phase^{14–16} and zeolites^{16–18} have been published.

Sodupe et al.¹⁵ studied the bonding of NO₂ to Cu and Ag using the MP2 and DFT methods in conjunction with moderate basis sets. The energy calculations were refined by MCPDF, CCSD(T), and QCISD(T) single point calculations. Three isomers of CuNO₂ were found¹⁵—the most stable C_{2v} bidentate η²-O,O isomer, the C_s monodentate η¹-O isomer, and the least stable C_{2v} monodentate η¹-N isomer. Only moderately sized basis sets of DZ quality were used in the study,¹⁵ and thus the calculated relative energies of the isomers differed significantly depending on the levels of approximation used. In some cases, also sizable differences (up to 24 kcal/mol) between CCSD(T) and QCISD(T) were obtained and attributed to an unsound estimation of the triple excitations.¹⁵ Similar conclusions had already been drawn for CuCH₃ by Frenking et al.¹⁹ who reported “dramatic failure” of the QCISD(T) method. However, it was shown later²⁰ that this failure of the QCISD(T) method, which is reflected in the flawed bond energy, is due to the inferiority of the QCISD method itself rather than due to the failure of

Corresponding author e-mail: stepan.sklenak@jh-inst.cas.cz.

the perturbative estimate of connected triple excitation contributions (T). It will be discussed later in this paper that the CuNO_2 and Cu^+NO_2 systems suffer from similar problems, and, in some cases, symmetry breaking leads to further problems in evaluation of physical-chemical properties.

Sauer et al.¹⁶ studied the structure and stability of Cu^+NO_2 in the gas phase and in the ZSM-5 zeolite using the B3LYP method. In the gas phase, they found three minima and two transition states on the ground state ($^2A'$ and 2A_1) potential energy surface of Cu^+NO_2 . The $\eta^1\text{-O}$ trans isomer was calculated to be the most stable species. The $\eta^1\text{-O}$ cis and $\eta^1\text{-N}$ isomers are higher in energy by 2 and 10 kcal/mol, respectively. Sauer et al.¹⁶ concluded that the bonding in Cu^+NO_2 is mainly noncovalent and arises from the interaction of the $^1S(d^{10})$ state of Cu^+ and the 2A_1 ground state of NO_2 . Further information on Cu^+NO_2 can be extracted from the recently appeared comparative study of Ducere et al.¹⁴ on the binding of NO_2 , NH_3 , H_2O , NO , N_2O , N_2 , and O_2 to Cu^+ and Cu^{2+} at several DFT and ab initio levels.

In the present paper we recalculate the $[\text{Cu}, \text{N}, \text{O}_2]^{0/+}$ neutral and positively charged systems at the uniform CCSD(T) level of theory with large ANO basis sets.^{21,22} These calculations serve for evaluating reliable relative stabilities and interconversion profiles as well as benchmarks for the most common DFT methods.

2. Methods

All the studied species were fully optimized, and the vibrational frequencies were determined using the MOLPRO ab initio program package²³ employing the Roos augmented ANO basis sets^{21,22} in the contractions designated as Basis-I (Cu: $21s15p10d6f/6s5p4d2f$ and O,N: $14s9p4d/4s3p2d$) and Basis-II (Cu: $21s15p10d6f4g/8s7p5d3f2g$ and O,N: $14s9p4d3f/5s4p3d2f$) and obtained from the Extensible Computational Chemistry Environment Basis Set Database, Version 02/25/04.²⁴

The ab initio calculations were performed at the two correlated ab initio CCSD(T)^{25–29} and QCISD(T)^{25,26,29,30} levels of theory as implemented in the MOLPRO program. The open shell species were calculated using the spin unrestricted (UCCSD(T)/ROHF^{31,32} and UQCISD(T)/ROHF^{31,32}) methods. Some supporting calculations were performed with the GAUSSIAN03 program package³³ at the UCCSD(T)/UHF level.

It was pointed out by Urban et al.^{34,35} that for the $\text{Cu}\cdots\text{OH}_2$ complex the triple excitations which follow from correlating the $3p^6$ shell of Cu make a considerable contribution in the vicinity of the minimum of the interaction potential. To investigate the effect of the $3p^6$ shell of Cu on the relative energies of the CuNO_2 and Cu^+NO_2 species, we carried out single point CCSD and CCSD(T) calculations. However, the results showed that the effect of the $3p$ electrons on the relative energies is in the range of a few tenths of kcal/mol. Thus we decided to use the “frozen core” approximation as implemented in the MOLPRO program, i.e., only the copper $3d$ and $4s$ electrons as well as $2s$ and

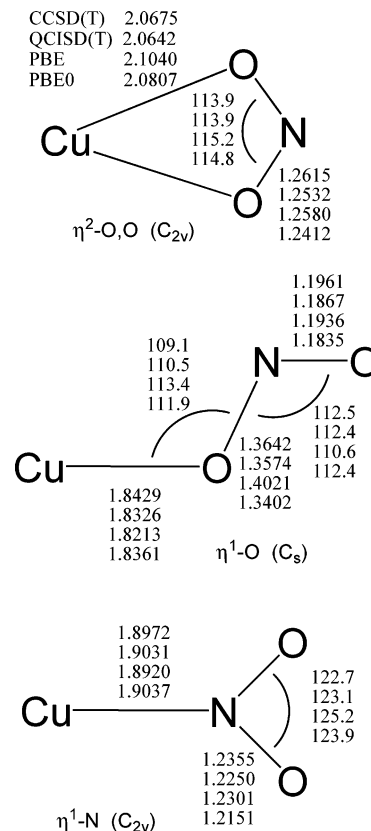


Figure 1. Optimized structures of the $\eta^2\text{-O,O}$ (a, top), $\eta^1\text{-O}$ (b, middle), and $\eta^1\text{-N}$ (c, bottom) isomers of CuNO_2 at CCSD(T)/Basis-II, QCISD(T)/Basis-II, PBE/Basis-II, and PBE0/Basis-II. Bond lengths are in Å and bond angles in deg.

$2p$ electrons of N and O were correlated in all the CCSD(T) and QCISD(T) calculations.

In addition, we also performed calculations using two pure and two hybrid density function theory methods—BPW91,³⁶ PBE³⁷ and PBE0,³⁸ B3LYP,^{39–41} respectively. The implementations of the unrestricted DFT methods were used for the open shell species. Moreover, the ACESII⁴² program was employed to test the stability of HF solutions and to calculate the CCSD(TQ)⁴³ energies as well as to obtain the CCSD amplitudes which were checked for all the species to ensure that the systems are well described by a single reference configuration.

3. Results and Discussion

3.1. CuNO_2 . 3.1.1. Relative Stabilities and Structures. We found three minima and two transition states connecting these minima on the $[\text{Cu}, \text{N}, \text{O}_2]$ potential energy surface. The optimized structures of all the species of CuNO_2 as well as of NO_2 and NO_2^- are given in Figure 1a–c and Tables S1 and S2 of the Supporting Information.

The C_{2v} bidentate $\eta^2\text{-O,O}$ isomer (Figure 1a) is calculated to be the most stable isomer of CuNO_2 at all levels of theory (see also Figure 2 and Table 1) and represents a pronounced well on the related PES. Only slight differences in the geometrical parameters can be observed depending on the method used. Not surprisingly, there is good agreement between the QCISD(T) and CCSD(T) results, since both methods are assumed to be more or less identical.^{44,45} The

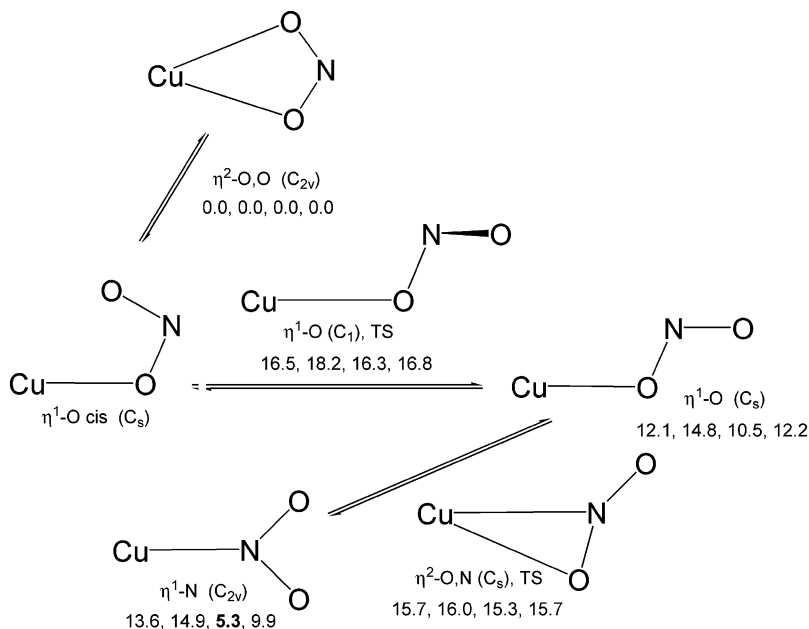


Figure 2. Relative energies (in kcal/mol) of the CuNO₂ isomers and transition states at CCSD(T)/Basis-II, QCISD(T)/Basis-II, PBE/Basis-II, and PBE0/Basis-II.

Table 1. Calculated Relative Energies (in kcal/mol) for All Minima and Transition States of CuNO₂^a

isomer	basis set	CCSD	CCSD(T)	QCISD	QCISD(T)	BPW91	PBE	PBE0	B3LYP
η^2 -O,O	Basis-I	0.0	0.0	0.0	0.0	0.0	0.0	0.0	0.0
η^2 -O,O	Basis-II	0.0	0.0	0.0	0.0	0.0	0.0	0.0	0.0
η^1 -N	Basis-I	15.3	14.2	14.1	16.0	5.3	5.4	10.1	9.2
η^1 -N	Basis-II	14.8	13.6	13.8	14.9	5.2	5.3	9.9	9.1
η^1 -O	Basis-I	11.4	11.6	9.3	15.2	10.0	10.5	12.3	10.8
η^1 -O	Basis-II	11.8	12.1	10.2	14.8	10.1	10.5	12.2	10.7
η^2 -O,N (TS)	Basis-I	16.9	16.2	16.7	16.6	15.0	15.2	15.8	15.9
η^2 -O,N (TS)	Basis-II	16.4	15.7	16.3	16.0	15.0	15.3	15.7	15.9
η^1 -O (TS)	Basis-I	15.6	16.1	14.7	18.3	16.2	16.6	17.2	15.7
η^1 -O (TS)	Basis-II	15.9	16.5	15.3	18.2	15.9	16.3	16.8	15.4

^a The energy values include the electronic energy and zero point energy (ZPE). For the CCSD and QCISD levels, the ZPE values at CCSD(T) and QCISD(T), respectively, are used.

largest CCSD and QCISD amplitudes (0.09 and 0.11) as well as the values of the T1 diagnostic (0.030 and 0.037) are small.

It should be noted that the pure DFT calculated Cu–O bond lengths are slightly longer (0.04 Å) than that at the CCSD(T) level, and the inclusion of the “exact HF exchange” in the hybrid methods brings the ab initio and DFT results closer (difference of 0.02 Å). It has been stated earlier that the bonding between Cu and NO₂ in the η^2 -O,O isomer is mainly ionic.¹⁵ This ionic character of the metal–ligand bond is reflected in the structure of the NO₂ moiety that is very close to that of NO₂[−] ($r(\text{N–O})$: 1.262 Å; $\alpha(\text{O–N–O})$: 116.4° at CCSD(T)/Basis-II) rather than to that of NO₂ ($r(\text{N–O})$: 1.198 Å; $\alpha(\text{O–N–O})$: 134.1° at CCSD(T)/Basis-II).

The remaining two isomers on the neutral [Cu, N, O₂] PES are close in energy, and their relative order of stabilities depends strongly on the level of theory used (see Figure 2 and Table 1). The C_s monodentate η^1 -O isomer (Figure 1b) is the second most stable species at CCSD(T). The copper acts as a monodentate ligand, and it is coordinated only to the oxygen atom. The calculated Cu–N distance (2.627 Å at CCSD(T)/Basis-II) is significantly longer than the bonding

distance, and, furthermore, also the orbital analysis reveals that there is no significant contribution of the Cu–N overlap to the bonding (vide infra). All the methods provided similar structures. The calculated Cu–O bond is uniformly shorter than that in the C_{2v} bidentate η^2 -O,O isomer reflecting a larger covalent contribution to the bonding. The only geometry parameter which significantly varies at the different levels is the O_{Cu}–N bond distance which spans the interval from 1.340 Å (PBE0/Basis-II) to 1.413 Å (BPW91/Basis-I). The O_{Cu}–N bond is significantly longer than the N=O bond (by 0.17 Å at CCSD(T)/Basis-II) which, consistently with the valence bond picture, has a character of a double bond rather than a single bond. The calculated O–N–O bond angle (113° at CCSD(T)/Basis-II) is again much closer to that of NO₂[−] than to that of NO₂. Thus, also in this η^1 -O isomer the bonding is dominated by the ionic character.

The C_{2v} monodentate η^1 -N isomer (Figure 1c) is calculated at CCSD(T) to be the least stable CuNO₂ isomer (Figure 2 and Table 1). The calculated structures are very similar at all the levels used. The calculated N–O bond length (1.236 Å at CCSD(T)/Basis-II) is shorter and the O–N–O bond angle (123° at CCSD(T)/Basis-II) is larger than the corre-

sponding geometry parameters of the C_{2v} bidentate η^2 -O,O isomer, and their values are between those of NO_2 and NO_2^- . This fact reveals that the covalent contribution to the bonding is larger for the η^1 -N isomer than for the other two isomers.

Although the η^2 -O,O isomer is the most stable species at all computational levels (see Table 1), the order of the two less stable isomers is different at various levels of approximation. Let us first focus on the coupled cluster (CC) level. The η^1 -O isomer is calculated to be less stable than η^2 -O,O by 11–12 kcal/mol, while the η^1 -N isomer is higher in energy than η^2 -O,O by 14–15 kcal/mol. The effects of the perturbative contributions of connected triple excitations (hereafter (T)) as well as of the size of the basis set are negligible in both cases (smaller than 1 kcal/mol).

The influence of the perturbative contributions of connected quadruple excitations (hereafter (Q)) on the relative energies of the isomers of CuNO_2 was investigated as well. However, the CCSD(TQ)/Basis-I//CCSD(T)/Basis-I results reveal that the effect of (Q) on the relative energies is very small—a few tenths of kcal/mol. [η^1 -O and η^1 -N are less stable than η^2 -O,O by 12.0 and 14.7 kcal/mol, respectively, at CCSD(TQ)/Basis-I//CCSD(T)/Basis-I (plus the ZPE energy at CCSD(T)/Basis-I).] The negligible effect of (Q) is in agreement with already small effect of the triples (T).

All three isomers of CuNO_2 were also calculated employing the effective core potential of Hay and Wadt⁴⁶ and Basis-I at the CCSD(T) level. However, the relative energies of the three isomers as well as their optimized geometries were very close to those calculated at the CCSD(T)/Basis-II//CCSD(T)/Basis-I level. [η^1 -O and η^1 -N are less stable than η^2 -O,O by 12.8 and 15.5 kcal/mol, respectively, at CCSD(T)/ECP+Basis-I//CCSD(T)/ECP+Basis-I (plus the ZPE energy at CCSD(T)/Basis-I).]

The energy order of the isomers of CuNO_2 can be also rationalized using a simple concept of electronegativity. The copper atom which donates one s electron to the NO_2 moiety prefers to coordinate to a more electronegative element, i.e., oxygen. Thus η^2 -O,O, in which Cu coordinates to two oxygen atoms, is the most stable. Consequently, the η^1 -O species is less stable (Cu is ligated only to one oxygen atom) followed by η^1 -N (Cu coordinates to the nitrogen atom).

3.1.2. Bonding. The analysis of the orbitals involved in the formation of the bond between Cu and NO_2 in the η^2 -O,O isomer of CuNO_2 (Figure S1 of the Supporting Information) reveals that the bonding between Cu and NO_2 in CuNO_2 is mainly ionic, and it arises from the interaction of the $^1\text{S}(d^{10})$ state of Cu^+ and the $^1\text{A}_1$ ground state of NO_2^- . The 4s orbital of Cu, which is singly occupied in Cu, interacts with the SOMO orbital ($6a_1$) of NO_2 to form the HOMO orbital ($13a_1$) of CuNO_2 , which polarizes toward the NO_2 moiety. The $7b_2$ and $6b_2$ orbitals of CuNO_2 arise from the antibonding and bonding, respectively, combinations between the $3d_{yz}$ orbital of Cu and the $4b_2$ orbital of the NO_2 moiety. The remaining 3d orbitals of Cu do not significantly interact with the orbitals of NO_2 . The bonding in the other two isomers is very similar. The Mulliken populations calculated for all three isomers (Table 2) confirm an ionic character of all three isomers.

The bonding in all three isomers is driven by the donation

Table 2. Mulliken Populations in the s, p, and d Orbitals of Cu, N, and O of CuNO_2

isomer	atom	s	p	d	charge
η^2 -O,O	Cu	6.18	12.10	9.98	+0.73
η^2 -O,O	O	3.86	4.61	0.03	-0.51
η^2 -O,O	N	3.64	2.77	0.26	+0.29
η^1 -O	Cu	6.21	12.10	9.94	+0.73
η^1 -O	O ₁	3.88	4.70	0.03	-0.62
η^1 -O	N	3.65	2.85	0.24	+0.22
η^1 -O	O ₂	3.86	4.42	0.05	-0.34
η^1 -N	Cu	6.18	12.06	9.93	+0.82
η^1 -N	N	3.58	2.93	0.36	+0.09
η^1 -N	O	3.86	4.54	0.04	-0.45

(ca 0.8 e) of the 4s-electron on copper to the NO_2 fragment. The back-donation from NO_2^- into the 4p orbitals of Cu is sizably smaller. This back-donation is the largest for the η^2 -O,O isomer, about 0.08 e, and it is smaller for η^1 -O (0.04 e) and negligible for η^1 -N.

3.1.3. QCISD. When analyzing the QCISD and QCISD(T) relative energies, notable differences (1–4 kcal/mol) between the QCI and CC values are found for the η^1 -O and η^1 -N species. Moreover, the effect of (T), which is small at CC, is sizable at QCI especially for η^1 -O as it increases the relative energy by 5–6 kcal/mol with respect to η^2 -O,O. Surprisingly, the energy gap between the CC and QCI results for η^1 -O and η^1 -N as obtained by Sodupe at al.,¹⁵ when using a smaller [Cu: 8s6p4d] basis set, were substantially larger (up to 24 kcal/mol). In the manner of "dramatic failure of QCISD(T)"^{15,19,47} this effect was attributed to the unsound estimation of (T) i.e., the perturbative method was made responsible for the failure. These explanations ignore the fact that already the QCISD solution is severely flawed,^{20,48} and the omitted nonzero connected T_1 -terms in the QCISD equations are fully responsible for these irregularities. Furthermore, the QCISD method offers no significant computational advantages with respect to CCSD and should be avoided.

3.1.4. DFT. The results obtained at DFT depend on whether the functional employed is pure (BPW91 and PBE) or hybrid (PBE0 and B3LYP). η^1 -O is calculated to be 10 kcal/mol less stable than η^2 -O,O with the pure DFT, while the hybrid DFT values are very close to the 12 kcal/mol calculated at CCSD(T)/Basis-II. The pure DFT relative energies of η^1 -N with respect to η^2 -O,O (5 kcal/mol) and even the 10 kcal/mol calculated at PBE0 and B3LYP are in very poor agreement with the superior CCSD(T) values (14 kcal/mol) irrespective of the similar optimized geometries of η^1 -N.

3.1.5. Transition States. Two transition states were localized on the potential energy surface of CuNO_2 . The first one is the C_1 monodentate η^1 -O species and the second one is the C_s bidentate η^2 -O,N species. The calculated imaginary frequencies reveal that the isomerizations η^2 -O,O \rightarrow η^1 -O and η^1 -O \rightarrow η^1 -N proceed via the former and latter transition states, respectively.

The calculations showed that all three bond distances of the C_1 η^1 -O TS are close to those of the C_s η^1 -O isomer for all the methods used. The relative energy of the η^1 -O TS,

Table 3. Bond Dissociation Energies (in kcal/mol) of the η^2 -O,O Isomer of CuNO₂ with Respect to the Cu + NO₂ and Cu⁺ + NO₂⁻ Channels

channel	basis set	CCSD	CCSD(T)	HF	QCISD	QCISD(T)	BPW91	PBE	PBE0	B3LYP
Cu + NO ₂	Basis-I	55.3	54.7	48.7	56.3	53.8	44.5	48.0	48.2	46.3
Cu + NO ₂	Basis-II	55.9	55.2	47.0	56.7	54.3	43.6	47.1	47.3	45.5
Cu ⁺ + NO ₂ ⁻	Basis-I	172.8	176.0	157.4	174.8	176.1	185.6	189.0	179.6	179.4
Cu ⁺ + NO ₂ ⁻	Basis-II	172.8	176.3	156.7	174.8	176.5	186.2	189.4	179.8	179.8

Table 4. Vertical and Adiabatic Ionization Potentials (in kcal/mol) of the η^2 -O,O Isomer of CuNO₂

type	basis set	CCSD	CCSD(T)	QCISD	QCISD(T)	BPW91	PBE	PBE0	B3LYP
vertical	Basis-I	234.0	231.3	236.2	251.6	225.3	226.5	230.4	230.7
vertical	Basis-II	236.0	233.6	238.3	251.4	224.7	225.9	229.7	230.0
adiabatic	Basis-I	200.6	202.0	201.7	201.9	205.0	206.7	203.7	205.0
adiabatic	Basis-II	202.8	204.5	203.8	204.4	204.2	205.9	202.6	204.1

which also corresponds to the barrier of isomerization η^2 -O,O \rightarrow η^1 -O, is 16–17 kcal/mol at CCSD(T) and DFT. The imaginary frequency corresponds to the torsion mode, and thus the transition state connects the η^1 -O cis and trans species. However, all computational attempts to localize a η^1 -O cis species led to the η^2 -O,O isomer. Restricted optimization scans indicated that the η^1 -O cis species is rather a shoulder on the potential energy surface and the barrier for its isomerization into η^2 -O,O is most likely very small.

The calculated geometry parameters of the C_s bidentate η^2 -O,N TS depend significantly on the methods employed. The DFT schemes provide the structures having the Cu–O bond too short (by up to 0.20 Å) and the Cu–N bond too long (by up to 0.15 Å) with respect to the CCSD(T) results. In other words, the isomerization η^1 -O \rightarrow η^1 -N is found to have a late transition state at the CC and QCI levels, while it has an early TS at DFT. The imaginary frequency corresponds to C–N and C–O asymmetric stretching mode. Surprisingly, the calculated relative energies of the η^2 -O,N TS are within a small interval 15–17 kcal/mol for all the methods used.

3.1.6. Bond Dissociation Energies. In Table 3 we present the bond dissociation energies, hereafter D_e , of the η^2 -O,O isomer of CuNO₂ with respect to Cu and NO₂ as well as to Cu⁺ and NO₂⁻. The D_e values calculated at CCSD(T) are 55 and 176 kcal/mol for the Cu + NO₂ and Cu⁺ + NO₂⁻ channels, respectively. The effect of (T) is 3 kcal/mol for the latter channel and negligible for the former one. The QCI D_e values are rather close to the CC ones. The differences between the CCSD(T) and HF D_e values reveal the effect of electron correlation which is 6–8 and 19 kcal/mol for the Cu + NO₂ and Cu⁺ + NO₂⁻ channels, respectively. The D_e values calculated at the hybrid DFT are significantly smaller by (7–10 kcal/mol) than those calculated at CCSD(T) for the Cu + NO₂ channel. The main reason of the disagreement is the inability of DFT to correctly describe the copper atom (2A_g). The Cu-ionization potential calculated at PBE0/Basis-II and B3LYP/Basis-II is about 7 and 11 kcal/mol larger, respectively, than that calculated at CCSD(T)/Basis-II. On the other hand, for the Cu⁺ + NO₂⁻ channel the agreement between the hybrid DFT and CCSD(T) D_e values is significantly better as the difference is about 3.5 kcal/mol.

The effect of the size of the basis set is less than 1 kcal/mol for all the methods employed.

3.1.7. Ionization Potentials. To complete the figure and to make a bridge to the charged species we calculated the vertical (IP_v) and adiabatic (IP_a) ionization potentials of the η^2 -O,O isomer of CuNO₂. The individual values are revealed in Table 4. The IP_v values calculated at the CCSD, CCSD(T), QCISD, and hybrid DFT levels lie in a narrow interval 230–238 kcal/mol. It should be noted that the QCISD(T) values are significantly larger.

In contrast to IP_v, all the methods used provide very similar adiabatic ionization potentials (201–207 kcal/mol) since the geometries of Cu⁺NO₂ are relaxed and the corresponding energies are calculated at the minimum points of the energy potential surface.

3.2. Cu⁺NO₂. 3.2.1. Relative Stabilities and Structures. Let us turn our attention on the positively charged system. We found three minima and two transition states connecting these minima on the potential energy surface. The optimized structures of all the species of Cu⁺NO₂ are given in Figure 3a–c and Table S3 of the Supporting Information.

The C_s monodentate η^1 -O trans isomer ($^2A'$) (Figure 3a) is calculated to be the most stable isomer of Cu⁺NO₂ at all levels of theory, see Figure 4 and Table 5. The CCSD(T), QCISD(T), and hybrid DFT methods provide very similar structures. The Cu–O bond length is calculated to be 1.985 and 1.96 Å at CCSD(T)/Basis-II and hybrid DFT/Basis-II. Due to the missing bonding electron, the bond is longer than the corresponding Cu–O bond in the η^1 -O isomer of CuNO₂ by 0.14 Å. On the other hand, the lengths of the N–O bonds of η^1 -O trans of Cu⁺NO₂ are significantly shorter than those of η^1 -O of CuNO₂ (1.239 and 1.166 Å for Cu⁺NO₂; 1.364 and 1.196 Å for CuNO₂), and they are together with the value of the O–N–O bond angle (132°) close to the geometry parameters of NO₂ (1.198 Å and 134°). The pure DFT methods provided significantly shorter Cu–O bond lengths (~1.90 Å).

The C_s monodentate η^1 -O cis isomer ($^2A'$) (Figure 3b) is calculated to be the second most stable minimum lying 2–3 kcal/mol at all the levels used (see Figure 4 and Table 5) higher than η^1 -O trans. The calculated geometry parameters of η^1 -O cis are very close to those of η^1 -O trans possessing

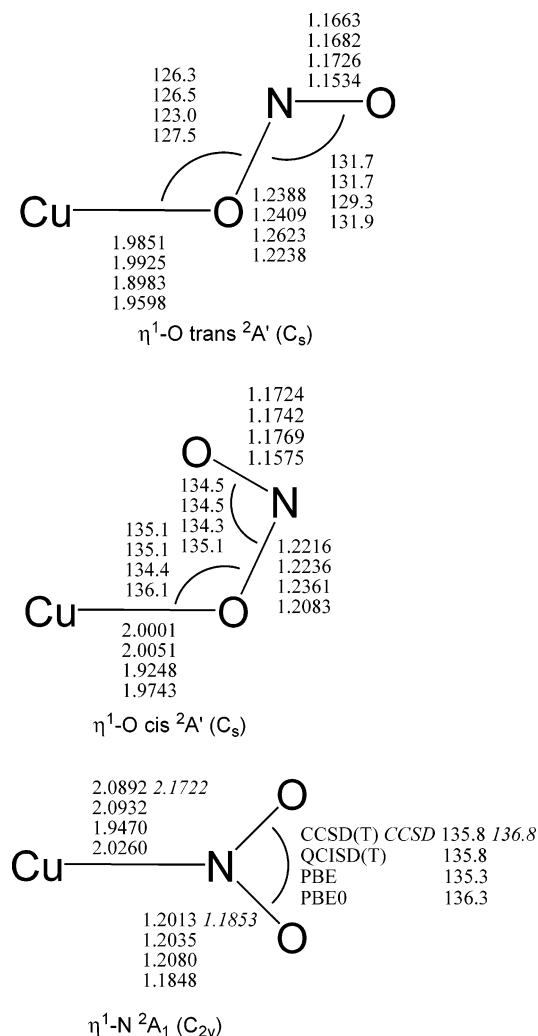
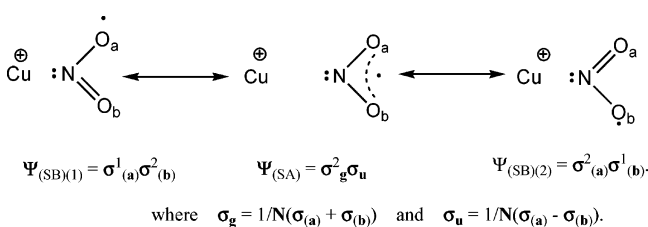


Figure 3. Optimized structures of the η^1 -O trans (a, top), η^1 -O cis (b, middle), and η^1 -N (c, bottom) isomers of Cu^+NO_2 at CCSD(T)/Basis-II, QCISD(T)/Basis-II, PBE/Basis-II, and PBE0/Basis-II. The values in italic are at CCSD/Basis-II (only for the η^1 -N isomer). Bond lengths are in Å and bond angles in deg.

the same trends for the methods used. It only might be mentioned that the O–N–O angle is slightly widened reflecting the steric (nonbonding) repulsion of the Cu^+ . The largest CCSD amplitudes (0.07) as well as the values of the T1 diagnostic (0.025) are very small for both isomers.

3.2.2. Symmetry Breaking. The C_{2v} monodentate η^1 -N isomer (2A_1) (Figure 3c) is calculated to be the least stable among the isomers of Cu^+NO_2 (see Figure 4 and Table 5) at all the levels used. This isomer can be described by two degenerate valence bond structures having the unpaired electron on either $\text{O}_{(a)}$ or $\text{O}_{(b)}$.



That indicates a possibility of symmetry broken Hartree–Fock (HF) solutions for this species.^{20,48–51} When the η^1 -N

isomer (2A_1) is calculated in the C_{2v} symmetry, the wave function $\Psi_{(\text{SA})}$ is symmetry adapted (hereafter SA), and it belongs to the A_1 irreducible representation. $\Psi_{(\text{SA})}$ covers the resonance between two solutions bearing the unpaired electron on either $\text{O}_{(a)}$ or $\text{O}_{(b)}$. The symmetry adaptation is a further constrain in a variational calculation, and it might consequently lead to a higher energy. To investigate whether the symmetry adapted wave function of the η^1 -N isomer (2A_1) is stable, the stability of the HF solution was tested. We could not directly test the stability of the ROHF wave function (as used in the CCSD(T) and QCISD(T) calculations), but we tested the corresponding SA UHF wave function. The stability tests reveal that the SA UHF wave function, which is only slightly spin contaminated ($\langle S^2 \rangle = 0.78$), has several UHF \rightarrow UHF instabilities. When the orbital rotations corresponding to the instabilities were applied to the SCF eigenvectors and the SCF calculation was repeated with these rotated vectors as the starting guess, a UHF solution lower in energy by 6.3 kcal/mol was found. However, the price for lowering the energy is a heavy spin contamination ($\langle S^2 \rangle = 1.08$). Moreover, the corresponding UHF wave function does not transform as the A_1 irreducible representation of the C_{2v} point group.

The localized (symmetry broken; hereafter SB) solutions lead to a lower energy in a variational calculation, but the wave functions $\Psi_{(\text{SB})(1)}$ and $\Psi_{(\text{SB})(2)}$ do not transform as the totally symmetric irreducible representation of the molecular point group. The energy differences between the symmetry adapted (SA) and localized (SB) solutions for the η^1 -N isomer (2A_1) are negligible at CCSD despite the fact that the underlying ROHF wave function is heavily affected ($\Delta E^{(\text{SA}-\text{SB})} = 4$ kcal/mol). [The localized solution was obtained by running a calculation at the ROHF level with the η^1 -N isomer (2A_1) having two unequal N–O bond lengths and using that SCF solution as the guess in the subsequent calculations with the η^1 -N isomer (2A_1) possessing the optimized C_{2v} structure. The localized (SB) solution at the ROHF level leads to a lower energy than the SA solution by 4 kcal/mol. However, at CCSD both SA and SB solutions provide essentially the same energy due to the robustness of the CCSD method and its low energy sensitivity on the underlying SCF orbitals.] The largest CCSD amplitude (0.07) is rather small indicating that the effect is not due to a multireference character. Also the calculated T1 diagnostic of 0.025 is very small. On the other hand, the QCISD energy difference between the SA and SB solutions is sizable ($\Delta E^{(\text{SA}-\text{SB})} = 3.5$ kcal/mol) indicating that the orbital rotations could not be removed (the largest amplitude is 0.10). However, it is noteworthy that the inclusion of (T) for both CCSD and QCISD leads to the SA energy which is lower than the SB one. This indicates that both solutions (CCSD(T) and QCISD(T)) are not very reliable in these cases. To partially eliminate the effect of symmetry breaking, the geometry of the η^1 -N isomer (2A_1) was reoptimized at the CCSD level of theory. Sizable changes in geometry are observed. The Cu–N bond is calculated to be longer by 0.08 Å at CCSD ($r(\text{Cu}-\text{N})$ is 2.200 Å and 2.172 Å at CCSD/Basis-I and CCSD/Basis-II, respectively) than at CCSD(T). The η^1 -N isomer (2A_1) is higher in energy than the η^1 -O

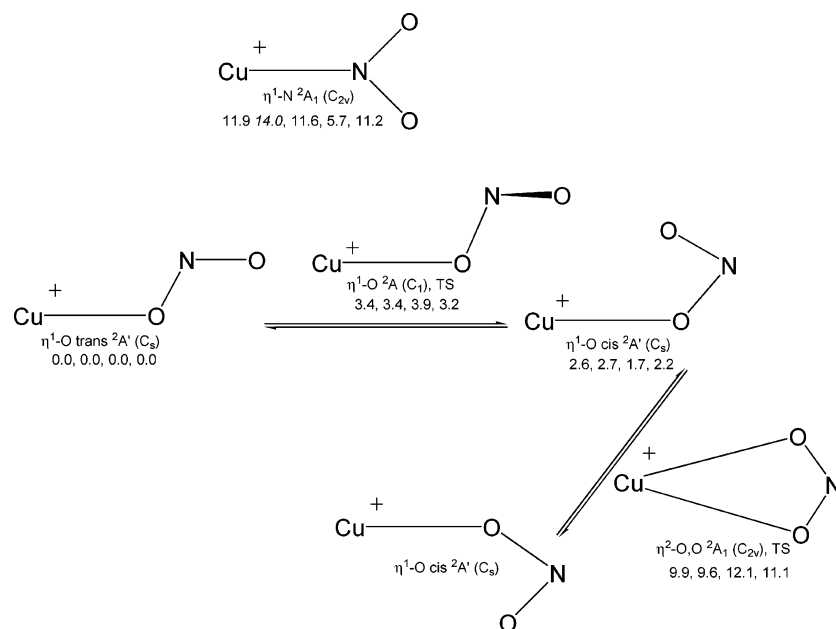


Figure 4. Relative energies (in kcal/mol) of the Cu⁺NO₂ isomers and transition states at CCSD(T)/Basis-II, QCISD(T)/Basis-II, PBE/Basis-II, and PBE0/Basis-II. The value in italic is at CCSD/Basis-II (only for the η^1 -N isomer).

Table 5. Calculated Relative Energies (in kcal/mol) for All Minima and Transition States of Cu⁺NO₂^a

isomer	state	basis set	CCSD	CCSD(T)	QCISD	QCISD(T)	BPW91	PBE	PBE0	B3LYP
η^1 -O trans	$^2A'$	Basis-I	0.0	0.0	0.0	0.0	0.0	0.0	0.0	0.0
η^1 -O trans	$^2A'$	Basis-II	0.0	0.0	0.0	0.0	0.0	0.0	0.0	0.0
η^1 -O cis	$^2A'$	Basis-I	2.4	2.6 ^b	2.7	2.7	1.9	1.8	2.2	2.3
η^1 -O cis	$^2A'$	Basis-II	2.4	2.6	2.6	2.7	1.7	1.7	2.2	2.2
η^1 -N	2A_1	Basis-I	14.2	12.2	15.3	11.9	5.6	5.5	11.0	11.0
η^1 -N	2A_1	Basis-II	14.0	11.9	14.9	11.6	5.8	5.7	11.2	11.3
η^2 -O,O (TS)	2A_1	Basis-I	9.7	9.7	10.1	9.4	11.7	11.7	10.5	11.2
η^2 -O,O (TS)	2A_1	Basis-II	9.8	9.9	10.2	9.6	12.1	12.1	11.1	11.6
η^1 -O (TS)	2A	Basis-I	3.1	3.4	3.5	3.4	4.2	4.2	3.5	3.7
η^1 -O (TS)	2A	Basis-II	3.0	3.4	3.3	3.4	3.9	3.9	3.2	3.4

^a The energy values include the electronic energy and zero point energy (ZPE). For the CCSD and QCISD levels, the ZPE values at CCSD(T) and QCISD(T) are used. The CCSD energies of the η^1 -N isomer correspond to the reoptimized geometry at CCSD. ^b 2.5 kcal/mol at CCSD(T)/ECP+Basis-II/CCSD(T)/ECP+Basis-I (plus the ZPE energy at CCSD(T)/Basis-I).

trans one by 14.0 kcal/mol at CCSD/Basis-II (11.9 kcal/mol at CCSD(T)/Basis-II).

3.2.2.1. CASSCF and MR-SDCI. To shed further light on the problem described above, we carried out CASSCF^{52–60} and subsequently internally contracted MR-SDCI^{61,62} calculations of the η^1 -N isomer (2A_1) of Cu⁺NO₂. Employing multireference methods such as CASSCF might be a way to avoid symmetry breaking^{63–66} since these methods include more reference functions which are able to better describe several valence bond structures. On the other hand, there is only a small amount of dynamic electron correlation included in the CASSCF calculations, and, thus, we enhanced the treatment using the MR-SDCI method.

Our single point CASSCF/Basis-I/CCSD/Basis-I calculations employed four different active spaces (in the reduced C_s symmetry) as described in Table 6. The symmetry adapted (SA) and broken (SB) HF wave functions were used as the initial guess for the CASSCF calculations. The SA guess led to a lower CASSCF energy than the SB guess (see the $\Delta E_{(SB-SA)}$ values in Table 6). The energy gap between the SB and SA CASSCF solutions ($\Delta E_{(SB-SA)}$) decreased as the size of the active space increased indicating that even this

CASSCF method is unable to guarantee a single solution when it is started from the SA and SB guesses. A larger active space should lead to a single solution (in the full CI limit); however, such calculations became prohibited for technical reasons. The corresponding CI vectors reveal that for all the active spaces used the CASSCF wave function is strongly dominated by an SCF-like solution based on the leading ground-state electron configuration. This fact causes that CASSCF does not provide a single solution for the SA and SB guesses; however, on the other hand, it justifies the use of the single reference CCSD method which yields the same energy for both SA and SB solutions. The involvement of a low-lying excited state of the η^1 -N isomer (2A_1) of Cu⁺NO₂ could be ruled out since the first excited state is some 70 kcal/mol higher in energy.

Further, we applied the MR-SDCI method employing the results of the CASSCF(7,8) and CASSCF(7,7) calculations in order to investigate the effect of dynamic electron correlation. The energy gap between the SA and SB solutions is reduced by only 0.2 kcal/mol at MR-SDCI, and it is further reduced by 0.8–0.9 kcal/mol when the Davidson correction⁶⁷ (MRCI(Q)) is employed (Table 6). However, the MRCI

Table 6. Energy Differences (in kcal/mol) between the Symmetry Adapted (SA) and Localized (SB) Solutions at Different Levels of Approximation for the η^1 -N Isomer (2A_1)^f

method ^a	active space orbitals	$\Delta E_{(SB-SA)}$	method	$\Delta E_{(SB-SA)}$	method	$\Delta E_{(SB-SA)}$
CASSCF(13,13)	16a' - 23a', 4a'' - 8a'' ^b	1.51				
CASSCF(13,12)	16a' - 22a', 4a'' - 8a'' ^c	1.59				
CASSCF(7,8)	19a' - 22a', 5a'' - 8a'' ^d	3.29	MRCI	3.07	MRCI(Q)	2.14
CASSCF(7,7)	19a' - 22a', 6a'' - 8a'' ^e	3.48	MRCI	3.27	MRCI(Q)	2.49
HF		-1.39				
CCSD		0.02				

^a CASSCF(*n,m*) where *n* is number of electrons and *m* is number of orbitals. ^b Frozen orbitals: 1a' - 15a', 1a'' - 3a''. ^c Frozen orbitals: 1a' - 15a', 1a'' - 3a''. ^d Frozen orbitals: 1a' - 18a', 1a'' - 4a''. ^e Frozen orbitals: 1a' - 18a', 1a'' - 5a''. ^f The geometry optimized at CCSD/Basis-I is used.

method (based on the chosen active space), unlike the single reference CCSD approach, is unable to guarantee a single solution. MR-SDCI does not include the T_1 excitations in an exponential form and thus does not exhibit a low sensitivity on the underlying orbitals.

A conclusion can be drawn from the presented results that in the case of symmetry breaking the CCSD is the method of choice if the following three conditions are fulfilled: First, the CCSD energy gap between SA and SB solutions should be small. Second, the corresponding CASSCF wave function is strongly dominated by the leading ground-state electron configuration, and finally, no low-lying excited state of the same symmetry as the ground state is present.

3.2.2.2. Symmetry Breaking and Vibrational Frequencies. The existence of symmetry broken solutions apparently causes problems in the numerical calculations of vibrational frequencies. Namely, one small imaginary frequency corresponding to the Cu-N-O bending mode was obtained at all the ab initio levels but CCSD as a consequence of the numerical evaluation of the frequencies in lower symmetry point groups. The CCSD frequency of the Cu-N-O bending mode is a real number for the step larger than 0.03 Å indicating that the η^1 -N species (2A_1) is a minimum on the potential energy surface. A smaller step leads to an imaginary value of the Cu-N-O wavenumber. The other five frequencies do not significantly depend on the step size.

3.2.2.3. Symmetry Breaking and DFT. The performance of DFT for symmetry breaking cases was a subject of several studies.⁶⁸⁻⁷² Head-Gordon et al.⁶⁸ studied three open shell systems (NO_3 , O_4^+ , and O_2^+) for which the UHF wave function breaks spatial symmetry. It was concluded⁶⁸ that symmetry broken solutions were obtained with DFT only when unusually large fractions of HF exchange (above 70%) were included into the hybrid functionals. The exchange was found more important than correlation in determining the tendency to preserve or break symmetry in DFT.⁶⁸ However, even when the optimization of Kohn-Sham orbitals leads to a symmetric solution, there is no guarantee that the vibrational frequencies will be entirely free of the effects of symmetry breaking because the higher-lying asymmetric solutions might strongly interact with the symmetric solution.⁶⁸ In addition, the MOLPRO program calculates DFT second derivatives numerically, and thus the calculated frequencies can suffer from the same problems as those obtained at CCSD.

To test whether the DFT methods used suffer from symmetry breaking for the η^1 -N isomer (2A_1) of Cu^+NO_2 , a

symmetry broken UHF solution was obtained and used as the guess in the subsequent calculations employing the UBWP91, UPBE, UPBE0, and UB3LYP methods for η^1 -N possessing the optimized C_{2v} structure. The calculations led to the symmetric solutions for all four DFT methods employing both basis sets. The subsequent evaluation of the vibrational frequencies provided only positive values.

The relative energies of η^1 -N are 11 and 6 kcal/mol at the hybrid and pure DFT levels (Figure 4), respectively. The former value is in agreement with the CCSD one (14 kcal/mol); however, the latter energy is once again unrealistically low.

The Cu-N bond length is calculated to be significantly shorter at PBE0 and B3LYP than at CCSD by some 0.15 Å and extremely shortened at BPW91 and PBE by about 0.25 Å. These results indicate that the pure DFT methods fail to provide correct structures and relative energies of η^1 -N. The Cu-N bond is significantly longer than the corresponding bond in the neutral $CuNO_2$. The N-O bond lengths as well as the O-N-O bond angle of η^1 -N are calculated to be close to the corresponding geometry parameters of NO_2 .

3.2.3. Bonding. The analysis of the orbitals involved in the formation of the bond between Cu^+ and NO_2 in the η^1 -O trans isomer of Cu^+NO_2 (Figure S2 of the Supporting Information) reveals that the bonding between Cu^+ and NO_2 in Cu^+NO_2 is ionic, and it arises from the interaction of the ${}^1S(d^{10})$ state of Cu^+ and the 2A_1 ground state of NO_2 . The prevailing interaction between Cu^+ and NO_2 is the electrostatic interaction. The 4s orbital of Cu, which is empty in Cu^+ , interacts with the SOMO orbital (10a') of NO_2 to form the SOMO orbital (20a') of $CuNO_2$ which very strongly polarizes toward the NO_2 moiety. The 19a' and 16a' orbitals of Cu^+NO_2 arise from the antibonding and bonding combinations, respectively, between the $3d_{x^2-y^2}$ orbital of Cu and the 9a' orbital of the NO_2 moiety. The Cu $3d_{xz}$ and NO_2 2a'' orbitals interact to form the antibonding 6a'' and bonding 4a'' orbitals of Cu^+NO_2 . The remaining 3d orbitals of Cu do not significantly interact with the orbitals of NO_2 . The bonding in the other two isomers is very similar. The Mulliken populations calculated for all three isomers (see Table 7) predict the positive charge being located predominantly on the copper center.

The Mulliken populations of 6.08, 12.06, and 9.97 e in the s, p, and d orbitals, respectively, of Cu of η^1 -O trans show a back-donation of 0.11 e from NO_2 to Cu. The back-donation for η^1 -O cis is very close to that of η^1 -O trans. On the contrary, there is no back-donation for η^1 -N.

Table 7. Mulliken Populations in the s, p, and d Orbitals of Cu, N, and O of Cu⁺NO₂

isomer	atom	s	p	d	charge
η^1 -O trans	Cu	6.08	12.06	9.97	+0.88
η^1 -O trans	O ₁	3.83	4.40	0.03	-0.27
η^1 -O trans	N	3.50	2.78	0.25	+0.44
η^1 -O trans	O ₂	3.85	4.15	0.05	-0.05
η^1 -O cis	Cu	6.07	12.05	9.98	+0.90
η^1 -O cis	O ₁	3.82	4.39	0.01	-0.24
η^1 -O cis	N	3.50	2.75	0.27	+0.44
η^1 -O cis	O ₂	3.85	4.20	0.05	-0.10
η^1 -N	Cu	6.02	12.01	9.97	+1.00
η^1 -N	N	3.50	2.89	0.30	+0.26
η^1 -N	O	3.85	4.23	0.05	-0.13

3.2.4. Transition States. Two transition states were localized on the potential energy surface of Cu⁺NO₂. The first one is the C₁ monodentate η^1 -O species (²A), and the second one is the C_{2v} bidentate η^2 -O,O species (²A₁). The calculated imaginary frequencies reveal that the former transition state connects the η^1 -O trans and η^1 -O cis isomers, while the latter TS connects two η^1 -O cis isomers. All computational attempts to find a transition state connecting the η^1 -O trans and η^1 -N isomers led to a η^2 -O,N structure which is very close in energy and geometry to the η^1 -N isomer. We assume that the calculated structure is an artifact of symmetry breaking rather than a real transition state. None of the chosen computational method is able to correctly calculate the curvature of the Cu⁺NO₂ potential energy surface in the vicinity of the minimum corresponding to the η^1 -N isomer due to symmetry breaking. It should be noted that the η^2 -O,N structure is very close to that found by Sauer et al.¹⁶ at B3LYP.

The calculations also showed that all three bond distances of the η^1 -O TS are close to those of the C_s η^1 -O trans and cis isomers for all the methods used. The imaginary frequency corresponds to the torsion mode. The relative energies of the η^1 -O TS, which also correspond to the barrier of isomerization η^1 -O trans → η^1 -O cis, are 3–4 kcal/mol at all the levels employed.

Since the C_{2v} bidentate η^2 -O,O TS (²A₁) is an open shell species having two equivalent N–O bonds, there is a possibility of symmetry broken HF solutions for this species. The stability of the symmetry adapted UHF wave function, which is only very slightly spin contaminated ($\langle S^2 \rangle = 0.77$), was tested, and an UHF → UHF instability was found. When the orbital rotations corresponding to the instabilities were applied to the SCF eigenvectors and the SCF calculation was repeated with these rotated vectors as the starting guess, an UHF solution having essentially the same energy was found. The corresponding $\langle S^2 \rangle$ value is 0.82 indicating a low-spin contamination of the wave function without an UHF → UHF instability. Since there is no change in energy between the two UHF solutions, we assume that the energy of the symmetry adapted ROHF solution is the same as that of the symmetry broken ROHF solution. The question is whether the imaginary frequency of the η^2 -O,O species (²A₁) indicates that the species is a transition state or it is an artifact caused by symmetry breaking. We assume that the former is the

case since the imaginary frequency is significantly larger (e.g. 173 cm⁻¹ at CCSD(T)/Basis-II) than that of the η^1 -N species (²A₁). In addition, the imaginary frequency is not sensitive to the method used, basis set and step size employed in the numerical calculations. Therefore, the η^2 -O,O species is a transition state connecting two η^1 -O cis isomers since the imaginary frequency corresponds to the asymmetric Cu–O stretching mode. The corresponding barrier is calculated to be 7–10 kcal/mol.

3.2.5. Bond Dissociation Energies. In Table 8 we present the bond dissociation energies (*D_e*) of the η^1 -O trans isomer of Cu⁺NO₂ with respect to Cu⁺ and NO₂. The CC, QCI, and hybrid DFT values of *D_e* are 22–24 kcal/mol. The pure DFT schemes provide the values of *D_e* which are larger by 3–5 kcal/mol. The differences between the CCSD(T) and HF *D_e* values reveal the effect of electron correlation which is 9 kcal/mol.

3.3. Infrared Frequencies. The calculated infrared frequencies are revealed in Table 9 (selected species at CCSD(T)) and Tables S4 (all isomers of CuNO₂; all levels), S5 (NO₂ and NO₂⁻; all levels), and S6 (the η^1 -O trans and cis isomers of Cu⁺NO₂; all levels) of the Supporting Information.

3.3.1. IR Frequencies of the η^2 -O,O Isomer of CuNO₂. Let us discuss the infrared frequencies of the most stable C_{2v} η^2 -O,O isomer of CuNO₂. The wavenumber of the Cu–O asymmetric stretching mode is calculated to be around 210 cm⁻¹ at CCSD(T), 190 cm⁻¹ at QCISD(T), 120 cm⁻¹ at pure DFT, and 160–180 cm⁻¹ at hybrid DFT. These values are scattered over a wider range (120–210 cm⁻¹) as compared to the symmetric mode due to the discussed problems with symmetry breaking of the HF solution. On the other hand, the symmetric Cu–O stretching mode (similarly the other symmetric ones), which does not suffer from symmetry breaking, is calculated to lie in a narrow range 290–330 cm⁻¹ at all the levels used. The O,O out-of-plane mode is the same case, and thus the wavenumber values span a small interval 350–380 cm⁻¹. The remaining three modes are more interesting for experimentalists, since their wavenumbers lie in a region which is experimentally easily accessible. The wavenumber of O–N–O bending mode is calculated to be 865 and 875 cm⁻¹ at CCSD(T)/Basis-I and CCSD(T)/Basis-II, respectively. The QCISD(T) values are greater by some 20 cm⁻¹. The DFT infrared frequencies of the O–N–O bending mode are close to the ab initio ones. The pure DFT methods provided slightly smaller wavenumbers (855 cm⁻¹), while the hybrid DFT methods gave somewhat greater wavenumbers (890–910 cm⁻¹).

The asymmetric (as) and symmetric (ss) N–O stretching modes (1262 and 1287 cm⁻¹, respectively, at CCSD(T)/Basis-II) are much closer to those of NO₂⁻ (1273 cm⁻¹ (as) and 1303 cm⁻¹ (ss)) than to those of NO₂ (1345 cm⁻¹ (ss) and 1666 cm⁻¹ (as); all values at CCSD(T)/Basis-II). This fact indicates an ionic character of the η^2 -O,O isomer (Cu⁺NO₂⁻). It should be noted, that the N–O stretching modes calculated at DFT are not in agreement with the CCSD(T) values since the asymmetric stretching mode has a greater wavenumber than the asymmetric one by 5–50 cm⁻¹ depending on the functional. There is only one available experimental frequency (1220 cm⁻¹) of the stretching N–O

Table 8. Bond Dissociation Energies (in kcal/mol) of the η^1 -O Trans Isomer of Cu^+NO_2 with Respect to the $\text{Cu}^+ + \text{NO}_2$ Channel

basis set	CCSD	CCSD(T)	HF	QCISD	QCISD(T)	BPW91	PBE	PBE0	B3LYP
Basis-I	22.0	23.0	13.5	23.0	22.7	26.3	29.1	23.5	24.2
Basis-II	21.4	22.5	13.3	22.4	22.3	26.7	29.5	23.9	24.6

Table 9. Calculated CCSD(T) Infrared Frequencies (in cm^{-1})

species	symmetry	basis set	B ₂	A ₁	B ₁	A ₁	B ₂	A ₁
			Cu–O as	Cu–O ss	OO out	O–N–O b	N–O as	N–O ss
$\text{CuNO}_2 \eta^2\text{-O,O}$	C_{2v}	Basis-I	203.4	326.1	346.1	864.7	1216.9	1251.9
$\text{CuNO}_2 \eta^2\text{-O,O}$	C_{2v}	Basis-II	208.4	330.8	346.7	874.6	1262.0	1286.7
species	symmetry	basis set	A''	A'	A'	A'	A'	A'
			torsion	Cu–O–N b	Cu–O s	O–N–O b	O _{Cu} –N s	N–O s
$\text{CuNO}_2 \eta^1\text{-O}$	C_s	Basis-I	132.5	139.0	413.2	764.6	905.3	1560.2
$\text{CuNO}_2 \eta^1\text{-O}$	C_s	Basis-II	127.8	138.9	421.9	799.7	952.6	1584.4
species	symmetry	basis set	B ₂	A ₁	B ₁	A ₁	A ₁	B ₂
			Cu–N–O b	Cu–N s	OO out	O–N–O b	N–O ss	N–O as
$\text{CuNO}_2 \eta^1\text{-N}$	C_{2v}	Basis-I	129.8	325.3	375.9	806.1	1304.6	1412.0
$\text{CuNO}_2 \eta^1\text{-N}$	C_{2v}	Basis-II	144.6	329.5	378.3	817.1	1339.3	1457.5
species	symmetry	basis set	A ₁			A ₁	B ₂	
			O–N–O b			N–O ss	N–O as	
NO_2	C_{2v}	Basis-I	749.7			1316.9	1622.3	
NO_2	C_{2v}	Basis-II	758.8			1345.1	1665.5	
NO_2^-	C_{2v}	Basis-I	776.4			1267.4	1218.5	
NO_2^-	C_{2v}	Basis-II	787.9			1302.7	1273.1	
species	symmetry	basis set	A'	A''	A'	A'	A'	A'
			Cu–O–N b	torsion	Cu–O s	O–N–O b	O _{Cu} –N s	N–O s
$\text{Cu}^+\text{NO}_2 \eta^1\text{-O trans}$	C_s	Basis-I	135.5	121.2	269.6	811.4	1223.2	1768.0
$\text{Cu}^+\text{NO}_2 \eta^1\text{-O trans}$	C_s	Basis-II	121.8	124.7	268.5	801.7	1256.4	1755.5
$\text{Cu}^+\text{NO}_2 \eta^1\text{-O cis}$	C_s	Basis-I	96.0	214.5	291.9	745.3	1294.8	1674.6
$\text{Cu}^+\text{NO}_2 \eta^1\text{-O cis}$	C_s	Basis-II	98.2	214.4	295.3	749.9	1321.8	1711.7

mode of CuNO_2 , which was determined in Ar matrices⁷³ and assigned to the asymmetric stretching mode.

To further investigate the disagreement between the CCSD(T) and DFT frequencies of the N–O stretching modes of the $\eta^2\text{-O,O}$ isomer of CuNO_2 , we calculated the infrared frequencies of NaNO_2 (Table S7 of the Supporting Information) for which there are available experimental spectra⁷⁴ in solid Ar (1293 cm^{-1} ss, 1223 cm^{-1} as, and 826 cm^{-1} bending for the $\eta^2\text{-O,O}$ isomer of NaNO_2). We performed calculations on NaNO_2 , and the results reveal that the CCSD(T), QCISD(T), and all DFT methods reproduce the right order of the N–O stretching modes of NaNO_2 . Based on these results we firmly believe that most likely the symmetric N–O stretching mode of the $\eta^2\text{-O,O}$ isomer of CuNO_2 has a greater wavenumber than the asymmetric one as predicted by the CCSD(T) and QCISD(T) methods.

3.3.2. IR Frequencies of Cu^+NO_2 . Let us look briefly at the two most stable isomers of Cu^+NO_2 (Table 9 and Table S6 of the Supporting Information). The calculated wavenumbers of the Cu–O–N bending mode are 110–130 cm^{-1} and 80–110 cm^{-1} , for trans and cis, respectively. The wavenumber of the torsion mode is significantly lower for trans (120–150 cm^{-1}) than cis (210–270 cm^{-1}). The

wavenumber of the Cu–O stretching mode is about 300 cm^{-1} for both isomers. The three modes involving the NO_2 moiety lie in a region which is experimentally easily accessible. The O–N–O bending mode is calculated to have a greater wavenumber for trans (750–810 cm^{-1}) than cis (700–760 cm^{-1}). The wavenumbers of the O_{Cu}–N and N–O stretching modes are very scattered, and thus an eventual assignment of experimental bands will be difficult. However, all the methods indicate that the wavenumber of N–O stretching is significantly larger than that of O_{Cu}–N due to the electrostatic interaction between Cu^+ and O_{Cu}.

4. Conclusions

In this paper, we have presented a computational study of CuNO_2 and Cu^+NO_2 at the CCSD(T), QCISD(T), and DFT levels of approximation. Several stationary points (minima and transition states) were located on the CuNO_2 and Cu^+NO_2 potential energy surfaces. We investigated the performance of the two pure (BPW91 and PBE) as well as two hybrid (PBE0 and B3LYP) DFT methods with respect to the superior CCSD(T) method. The hybrid DFT methods are superior to the pure DFT and predict the geometries and relative stabilities which are close to the CCSD(T) results

for the most of the species. However, the PBE0 and B3LYP calculated relative energies of the η^1 -N isomer of CuNO₂ are smaller by 4–5 kcal/mol compared to the CCSD(T) value, and, moreover, both methods also predict the bond dissociation energies of CuNO₂ (for the Cu + NO₂ channel) which differ as much as 10 kcal/mol from the CCSD(T) values. The sizable differences between the CCSD(T) and QCISD(T) results were analyzed. We showed that the inferiority of the QCISD method itself with respect to CCSD is responsible for the failures not just the unsound estimation of the triple excitations (T). The issue of symmetry breaking was investigated, and it was demonstrated that in the case of symmetry breaking CCSD is the method of choice.

Acknowledgment. This work was financially supported by the project “Information Society” No. 1ET400400413 (“Development of a program environment for mathematic simulations and predictions in catalysis and electrocatalysis”). We would also like to thank Dr. Jiří Pittner for helpful discussions on quantum chemistry methods.

Supporting Information Available: Calculated bond lengths and angles of all calculated species of CuNO₂ (Table S1), of NO₂ and NO₂⁻ (Table S2), and of all calculated species of Cu⁺NO₂ (Table S3); schematic diagram of the most important orbitals involved in the formation of the η^2 -O,O isomer of CuNO₂ (Figure S1) and of the η^1 -O trans isomer of Cu⁺NO₂ (Figure S2); calculated infrared frequencies and intensities of CuNO₂ (Table S4), of NO₂ and NO₂⁻ (Table S5), and of Cu⁺NO₂ (Table S6); and calculated infrared frequencies of the η^2 -O,O isomer of NaNO₂ (Table S7). This material is available free of charge via the Internet at <http://pubs.acs.org>.

References

- Wichterlova, B.; Sobalik, Z.; Dedecek, J. *Appl. Catal., B* **2003**, *41*, 97–114.
- Shelef, M. *Chem. Rev.* **1995**, *95*, 209–225.
- Kuroda, Y.; Iwamoto, M. *Top. Catal.* **2004**, *28*, 111–118.
- Yahiro, H.; Iwamoto, M. *Appl. Catal., A* **2001**, *222*, 163–181.
- Iwamoto, M.; Yahiro, H.; Torikai, Y.; Yoshioka, T.; Mizuno, N. *Chem. Lett.* **1990**, 1967–1970.
- Kucherov, A. V.; Kucherova, T. N.; Slinkin, A. A. *Catal. Lett.* **1991**, *10*, 289–296.
- Petunchi, J. O.; Sill, G.; Hall, W. K. *Appl. Catal., B* **1993**, *2*, 303–321.
- Wichterlova, B.; Sobalik, Z.; Skokanek, M. *Appl. Catal. A* **1993**, *103*, 269–280.
- Iwamoto, M.; Yahiro, H.; Tanda, K.; Mizuno, N.; Mine, Y.; Kagawa, S. *J. Phys. Chem.* **1991**, *95*, 3727–3730.
- Li, Y. J.; Hall, W. K. *J. Catal.* **1991**, *129*, 202–215.
- Spoto, G.; Zecchina, A.; Bordiga, S.; Ricchiardi, G.; Martra, G.; Leofanti, G.; Petrini, G. *Appl. Catal., B* **1994**, *3*, 151–172.
- Wichterlova, B.; Dedecek, J.; Sobalik, Z.; Vondrova, A.; Klier, K. *J. Catal.* **1997**, *169*, 194–202.
- Hitchman, M. A.; Rowbottom, G. L. *Coord. Chem. Rev.* **1982**, *42*, 55–132.
- Ducere, J. M.; Goursot, A.; Berthomieu, D. *J. Phys. Chem. A* **2005**, *109*, 400–408.
- Rodriguez-Santiago, L.; Branchadell, V.; Sodupe, M. *J. Chem. Phys.* **1995**, *103*, 9738–9743.
- Rodriguez-Santiago, L.; Sierka, M.; Branchadell, V.; Sodupe, M.; Sauer, J. *J. Am. Chem. Soc.* **1998**, *120*, 1545–1551.
- Sierraalta, A.; Anez, R.; Brussin, M. R. *J. Phys. Chem. A* **2002**, *106*, 6851–6856.
- Sierraalta, A.; Anez, R.; Brussin, M. R. *J. Catal.* **2002**, *205*, 107–114.
- Bohme, M.; Frenking, G. *Chem. Phys. Lett.* **1994**, *224*, 195–199.
- Hrušák, J.; Tenno, S.; Iwata, S. *J. Chem. Phys.* **1997**, *106*, 7185–7192.
- Pouamerigo, R.; Merchan, M.; Nebotgil, I.; Widmark, P. O.; Roos, B. O. *Theor. Chim. Acta* **1995**, *92*, 149–181.
- Widmark, P. O.; Malmqvist, P. A.; Roos, B. O. *Theor. Chim. Acta* **1990**, *77*, 291–306.
- MOLPRO, a package of ab initio programs designed by H.-J. Werner and P. J. Knowles; version 2002.1; R. D. Amos; A. Bernhardsson; A. Berning; P. Celani; D. L. Cooper; M. J. O. Deegan; A. J. Dobyn; F. Eckert; C. Hampel; G. Hetzer; P. J. Knowles; T. Korona; R. Lindh; A. W. Lloyd; S. J. McNicholas; F. R. Manby; W. Meyer; M. E. Mura; A. Nicklass; P. Palmieri; R. Pitzer; G. Rauhut; M. Schütz; U. Schumann; H. Stoll; A. J. Stone; R. Tarroni, T. Thorsteinsson; H.-J. Werner.
- Extensible Computational Chemistry Environment Basis Set Database; Version 02/25/04; the Molecular Science Computing Facility; Environmental and Molecular Sciences Laboratory; the Pacific Northwest Laboratory; Richland, WA 99352.
- Hampel, C.; Peterson, K. A.; Werner, H. J. *Chem. Phys. Lett.* **1992**, *190*, 1–12.
- Scuseria, G. E.; Schaefer, H. F. *J. Chem. Phys.* **1989**, *90*, 3700–3703.
- Scuseria, G. E.; Janssen, C. L.; Schaefer, H. F. *J. Chem. Phys.* **1988**, *89*, 7382–7387.
- Purvis, G. D.; Bartlett, R. J. *J. Chem. Phys.* **1982**, *76*, 1910–1918.
- Raghavachari, K. *J. Chem. Phys.* **1985**, *82*, 4607–4610.
- Pople, J. A.; Headgordon, M.; Raghavachari, K. *J. Chem. Phys.* **1987**, *87*, 5968–5975.
- Knowles, P. J.; Hampel, C.; Werner, H. J. *J. Chem. Phys.* **1993**, *99*, 5219–5227.
- Watts, J. D.; Gauss, J.; Bartlett, R. J. *J. Chem. Phys.* **1993**, *98*, 8718–8733.
- Gaussian 03; Revision C.02*; M. J. Frisch; G. W. Trucks; H. B. Schlegel; G. E. Scuseria; M. A. Robb; J. R. Cheeseman; J. A. Montgomery, J.; T. Vreven; K. N. Kudin; J. C. Burant; J. M. Millam; S. S. Iyengar; J. Tomasi; V. Barone; B. Mennucci; M. Cossi; G. Scalmani; N. Rega; G. A. Petersson; H. Nakatsuji; M. Hada; M. Ehara; K. Toyota; R. Fukuda; J. Hasegawa; M. Ishida; T. Nakajima; Y. Honda; O. Kitao; H. Nakai; M. Klene; X. Li; J. E. Knox; H. P. Hratchian; J. B. Cross; V. Bakken; C. Adamo; J. Jaramillo; R. Gomperts; R. E. Stratmann; O. Yazyev; A. J. Austin; R. Cammi; C. Pomelli; J. W. Ochterski; P. Y. Ayala; K. Morokuma; G. A. Voth; P. Salvador; J. J. Dannenberg; V. G. Zakrzewski; S. Dapprich; A. D. Daniels; M. C. Strain;

- O. Farkas; D. K. Malick; A. D. Rabuck; K. Raghavachari; J. B. Foresman; J. V. Ortiz; Q. Cui; A. G. Baboul; S. Clifford; J. Cioslowski; B. B. Stefanov; G. Liu; A. Liashenko; P. Piskorz; I. Komaromi; R. L. Martin; D. J. Fox; T. Keith; M. A. Al-Laham; C. Y. Peng; A. Nanayakkara; M. Challacombe; P. M. W. Gill; B. Johnson; W. Chen; M. W. Wong; C. Gonzalez; J. A. Pople. Gaussian, Inc.: Wallingford, CT, 2004.
- (34) Antusek, A.; Urban, M.; Sadlej, A. J. *J. Chem. Phys.* **2003**, *119*, 7247–7262.
- (35) Urban, M.; Sadlej, A. J. *J. Chem. Phys.* **2000**, *112*, 5–8.
- (36) Perdew, J. P.; Chevary, J. A.; Vosko, S. H.; Jackson, K. A.; Pederson, M. R.; Singh, D. J.; Fiolhais, C. *Phys. Rev. B: Condens. Matter Mater. Phys.* **1992**, *46*, 6671–6687.
- (37) Perdew, J. P.; Burke, K.; Ernzerhof, M. *Phys. Rev. Lett.* **1996**, *77*, 3865–3868.
- (38) Adamo, C.; Barone, V. *J. Chem. Phys.* **1999**, *110*, 6158–6170.
- (39) Becke, A. D. *J. Chem. Phys.* **1993**, *98*, 5648–5652.
- (40) Miehlich, B.; Savin, A.; Stoll, H.; Preuss, H. *Chem. Phys. Lett.* **1989**, *157*, 200–206.
- (41) Lee, C. T.; Yang, W. T.; Parr, R. G. *Phys. Rev. B: Condens. Matter Mater. Phys.* **1988**, *37*, 785–789.
- (42) Bartlett, R. J. ACESII is a program product of the Quantum Theory Project of University of Florida.
- (43) Bartlett, R. J.; Watts, J. D.; Kucharski, S. A.; Noga, J. *Chem. Phys. Lett.* **1990**, *165*, 513–522.
- (44) Paldus, J.; Cizek, J.; Jeziorski, B. *J. Chem. Phys.* **1989**, *90*, 4356–4362.
- (45) Paldus, J.; Cizek, J.; Jeziorski, B. *J. Chem. Phys.* **1990**, *93*, 1485–1486.
- (46) Hay, P. J.; Wadt, W. R. *J. Chem. Phys.* **1985**, *82*, 270–283.
- (47) Luna, A.; Alcamí, M.; Mo, O.; Yanez, M. *Chem. Phys. Lett.* **2000**, *320*, 129–138.
- (48) Lynch, B. J.; Truhlar, D. G. *Chem. Phys. Lett.* **2002**, *361*, 251–258.
- (49) Hrušák, J.; Iwata, S. *J. Chem. Phys.* **1997**, *106*, 4877–4888.
- (50) Dunietz, B. D.; Head-Gordon, M. *J. Phys. Chem. A* **2003**, *107*, 9160–9167.
- (51) Einfeld, W.; Morokuma, K. *J. Chem. Phys.* **2000**, *113*, 5587–5597.
- (52) Werner, H. J.; Knowles, P. J. *J. Chem. Phys.* **1985**, *82*, 5053–5063.
- (53) Knowles, P. J.; Werner, H. J. *Chem. Phys. Lett.* **1985**, *115*, 259–267.
- (54) Feller, D. F.; Schmidt, M. W.; Ruedenberg, K. *J. Am. Chem. Soc.* **1982**, *104*, 960–967.
- (55) Siegbahn, P. E. M.; Almlof, J.; Heiberg, A.; Roos, B. O. *J. Chem. Phys.* **1981**, *74*, 2384–2396.
- (56) Roos, B. O.; Taylor, P. R. *Chem. Phys.* **1980**, *48*, 157–173.
- (57) Lam, B.; Schmidt, M. W.; Ruedenberg, K. *J. Phys. Chem.* **1985**, *89*, 2221–2235.
- (58) Ruedenberg, K.; Schmidt, M. W.; Gilbert, M. M.; Elbert, S. T. *Chem. Phys.* **1982**, *71*, 41–49.
- (59) Ruedenberg, K.; Schmidt, M. W.; Gilbert, M. M. *Chem. Phys.* **1982**, *71*, 51–64.
- (60) Ruedenberg, K.; Schmidt, M. W.; Gilbert, M. M.; Elbert, S. T. *Chem. Phys.* **1982**, *71*, 65–78.
- (61) Werner, H. J.; Knowles, P. J. *J. Chem. Phys.* **1988**, *89*, 5803–5814.
- (62) Knowles, P. J.; Werner, H. J. *Chem. Phys. Lett.* **1988**, *145*, 514–522.
- (63) Davidson, E. R.; Borden, W. T. *J. Phys. Chem.* **1983**, *87*, 4783–4790.
- (64) Engelbrecht, L.; Liu, B. *J. Chem. Phys.* **1983**, *78*, 3097–3106.
- (65) Feller, D.; Huyser, E. S.; Borden, W. T.; Davidson, E. R. *J. Am. Chem. Soc.* **1983**, *105*, 1459–1466.
- (66) McLean, A. D.; Lengsfeld, B. H.; Pacansky, J.; Ellinger, Y. *J. Chem. Phys.* **1985**, *83*, 3567–3576.
- (67) Langhoff, S. R.; Davidson, E. R. *Int. J. Quantum Chem.* **1974**, *8*, 61.
- (68) Sherrill, C. D.; Lee, M. S.; Head-Gordon, M. *Chem. Phys. Lett.* **1999**, *302*, 425–430.
- (69) Harju, A.; Rasanen, E.; Saarikoski, H.; Puska, M. J.; Nieminen, R. M.; Niemela, K. *Phys. Rev. B: Condens. Matter Mater. Phys.* **2004**, *69*.
- (70) Corral, I.; Mo, O.; Yanez, M. *Int. J. Quantum Chem.* **2003**, *91*, 438–445.
- (71) Cohen, R. D.; Sherrill, C. D. *J. Chem. Phys.* **2001**, *114*, 8257–8269.
- (72) Russ, N. J.; Crawford, T. D.; Tschumper, G. S. *J. Chem. Phys.* **2004**, *120*, 7298–7306.
- (73) Worden, D.; Ball, D. W. *J. Phys. Chem.* **1992**, *96*, 7167–7169.
- (74) Lo, W. J.; Shen, M. Y.; Yu, C. H.; Lee, Y. P. *J. Chem. Phys.* **1996**, *104*, 935–941.